 doi:10.20944/preprints202208.0097.v1

Article

Acoustic Emission Monitoring of Atmospheric Corrosion on Aluminum Aircraft Structures at Varying Relative Humidity

Thomas Erlinger [1,*], Christoph Kralovec [1] and Martin Schagerl [1]

[1] Institute of Structural Lightweight Design, Johannes Kepler University Linz, Altenberger Str. 69, 4040 Linz, Austria; christoph.kralovec@jku.at (C.K.); martin.schagerl@jku.at (M.S.)
* Correspondence: thomas.erlinger@jku.at

Abstract: Atmospheric corrosion of aluminum aircraft structures occurs due to numerous reasons. A typical phenomenon leading to corrosion is the deliquescence of contaminants such as salts due to changes in relative humidity (RH) caused by aircraft operation at different altitudes and climate zones. Currently, corrosion of aircrafts is controlled by scheduled inspections. In contrast, the present contribution aims for a continuous monitoring approach by using the acoustic emission (AE) method to detect and further evaluate atmospheric corrosion. The AE method is frequently used for corrosion detection at typically immersion-like conditions or for corrosion types where stress-induced cracking is involved. However, it has not yet been demonstrated for atmospheric corrosion at unloaded aluminum structures. To address this question, the present investigation uses small droplets of a corrosive sodium chloride (NaCl) solution to induce atmospheric corrosion on aluminum alloy AA2024-T351. Operating conditions of an aircraft are simulated by a controlled variation in RH. In addition, videos of the corrosion site are recorded to visually observe the corrosion process. Pitting corrosion is generated and clearly measurable AE signals are detected. An automatic video processing algorithm looking for sudden changes on the corrosion site mainly detects hydrogen bubbles formed when aluminum reacts with aqueous solutions. A clear correlation between the observed pitting corrosion, the AE and the hydrogen bubble activity and the RH, i.e., the electrolyte present at the aluminum surface, is found. Thus, the findings demonstrate the applicability of the AE method for monitoring atmospheric corrosion of aluminum aircraft structures by today's measurement equipment. Numerous potential effects that can cause measurable AE signals are investigated and discussed. Among these, bubble activity is clearly considered to be the most emissive one.

Keywords: acoustic emission; atmospheric corrosion; aluminum; aircraft structure; pitting corrosion; hydrogen bubbles; structural health monitoring

1. Introduction

Corrosion of aluminum is a considerable issue to be kept under control in the aircraft industry to ensure safety and functionality of mechanical structures during operation. Due to its lightweight properties, aluminum is widely used for structural components of aircrafts. These can be exposed to various corrosive environments during operation. Common sources or corrosion promoting environments in the aircraft industries are aqueous electrolytes like sea spray in coastal regions or at flight over the ocean at low altitudes, system leaks of fluids as e.g., hydraulic oils or coolant fluids but also spillages inside the cabin like soups, coffee or mineral water can cause corrosion [1–4]. Furthermore, moisture from rain, fog or snow may form together with different pollutants like dirt, exhaust gases, sulfates, chlorides etc. electrically conductive and chemically reactive solutions that corrode aluminum [2]. If soluble salt contaminants are present and the relative humidity (RH) is above the deliquescence relative humidity (DRH) of the particular salt contamination, the salt takes up water from the ambient atmosphere and forms a highly concentrated electrolyte [5]. Aircrafts operate in different climate zones and altitudes, hence they are exposed to fast changes in temperature and RH which can lead to condensation and in combination with salts or other contaminats to a corrosive solution [1–3,6]. Except to leakage and spillages of larger amounts of electrolytes, the above mentioned examples are

 doi:10.20944/preprints202208.0097.v1

typical sources of so-called atmospheric corrosion, which is the corrosion of a metal where the electrolyte is present in the form of a thin film, small droplets, or both [1,5,6].

Typically, corrosion of structural components of aircrafts is kept under control by scheduled inspections and clear protocols on how to determine corrosion [3,7]. However, several research works can be found where corrosion issues of different industries are addressed by the use of non-destructive testing (NDT) and structural health monitoring (SHM) methods. For example, electrochemical techniques like the electrochemical noise technique, where the fluctuations of the electrochemical current or potential due to corrosion are analyzed [8], show good potential for corrosion monitoring [9]. There are also methods based on the electrochemical impedance spectroscopy which have already been tested in field applications several years ago [10]. Another group of monitoring methods are optical fiber based techniques. Principally, these techniques use changes in light characteristics, like frequency, phase shift, polarization or intensity caused by changes in strain, temperature, refractive index, pH-value, chloride content, etc. [11]. Several research can be found in civil engineering for corrosion monitoring of reinforced concrete, where e.g., the formation of corrosion products causes measurable changes in strain, temperature or the refractive index of fiber optic sensors [12]. But fiber optic techniques have also been tested for aircrafts [13,14], e.g., by using fluorescent fiber optic sensors that detect aluminum ions from early stages of corrosion. Besides the already mentioned methods also acoustic methods are of big importance in corrosion monitoring. The most popular technique in this context perhaps is ultrasonic testing (UT) [15]. UT is well developed for ground based NDT applications during scheduled maintenance of aircraft components. Further acoustic methods for corrosion monitoring are guided waves (GW) and acoustic emission (AE). GW is an active method that uses transducers to send defined burst signals into the structure under investigation and evaluates the changes and reflections of the acoustic waves resulting from interaction with a potential damage. Whereas AE is a passive method that measures acoustic waves that are directly caused by the formation or presence of a damage. Both, GW and AE seem to be promising methods for automated corrosion monitoring [16,17].

Especially, the AE technique has attracted attention for monitoring of corrosion of metals in recent years. AE is a passive method that detects the rapid release of energy in the form of a transient elastic waves traveling through a monitored structure. Typical applications of AE can be found in detecting and monitoring of structural damages like cracks, impact events and delamination in different kinds of mechanical structures [18]. However, there are also numerous research works and industrial applications for corrosion detection and monitoring by AE. For example, AE is used in the petroleum and natural gas industry for leakage and corrosion detection of large tanks and pipelines made of different steels [19,20]. Another sector where AE is used is in civil engineering for corrosion monitoring of steel-reinforced concrete [21,22]. In contrast to steel, to the authors' best knowledge no industrial applications and only little research work can be found dealing with AE monitoring of corrosion of aluminum.

In [23] for example pitting corrosion of aluminum alloy AA2024 is analyzed by accelerated corrosion tests using potentiostatic polarization, [24] investigates exfoliation corrosion of AA2024 and AA7449 aluminum alloys and [25] pitting corrosion of an AA1050 aluminum alloy by potentiodynamic polarization. The found research works use immersion-like setups for their investigations, i.e., a large volume of electrolyte is in contact with the specimen. Aluminum reacts under hydrogen (H_2) formation when it comes into contact with aqueous solutions [6,26,27], thus, at immersion tests H_2 bubbles can be observed clearly. The research works mentioned above, always concluded that the most emissive sources are related to H_2 formation and the evolution of its bubbles. Consequently, it is expected that AE can detect corrosion as soon as the first H_2 bubbles appear, and thus, has the potential to detect corrosion earlier than other acoustic methods. Summarized, it is already been shown that corrosion of aluminum can be detected with AE. However, this formation of H_2 bubbles may not exist or may be very small in atmospheric corrosion due

Preprints (www.preprints.org) | NOT PEER-REVIEWED | Posted: 4 August 2022 doi:10.20944/preprints202208.0097.v1

to the small amount of electrolyte involved. Therefore, AE might not be applicable at all to atmospheric corrosion, or it might have limited applicability with current measurement equipment. Although the authors conducted an extensive literature review, no research was found that demonstrates this applicability.

The present contribution investigates whether atmospheric corrosion, typical for the operating conditions of aluminum aircraft structures, can be detected with the AE method. Therefore, a small droplet of electrolyte is used to trigger corrosion at a specimen and the RH is controlled to simulate periodic drying and wetting due to condensation. Aluminum alloy AA2024-T351 which is commonly used in the aircraft industry [1,6,26,27], is used for the investigation. Alloys of the 2XXX series are sensitive to localized corrosion in the form of pitting corrosion, intergranular corrosion, exfoliation corrosion and also stress corrosion cracking [6]. In atmospheric corrosion environments and the absence of mechanical loading, the most occurring form is pitting corrosion, which is further enhanced when chlorides (Cl^-) are present in the corrosive atmosphere [6]. Figure 1 illustrates the mechanism of pitting corrosion under a droplet of an aqueous solution and H_2 bubble activity, which can be divided into the phases ① formation of the H_2 bubble, ② detachment from the metal surface and movement of the bubble in the droplet, ③ arrival of the bubble at the droplet surface and bubble growth and ④ bursting of the bubble. Pitting corrosion follows two

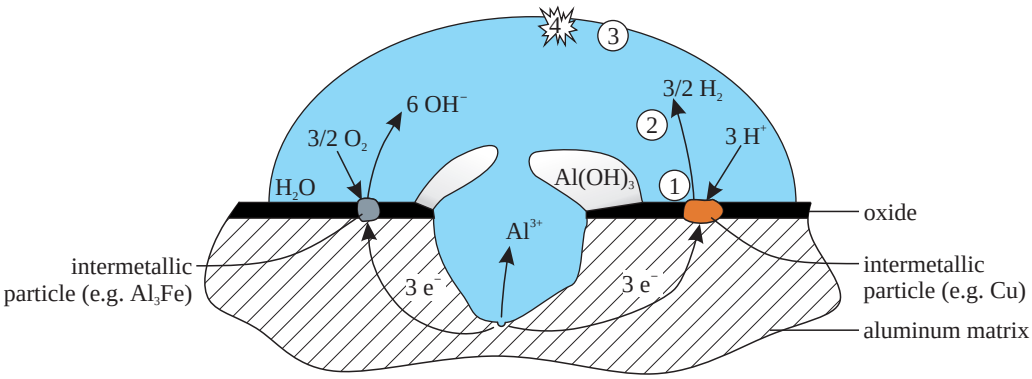

Figure 1. Mechanism of pitting corrosion of aluminum under a droplet of an aqueous solution [6]. H_2 bubble activity is distinguished into ① formation , ② detachment from metal surface and movement, ③ arrival at droplet surface and growth and ④ bursting of H_2 bubbles.

electrochemical reactions, anodic oxidation at the base of the pit

$$\mathrm{Al} \longrightarrow \mathrm{Al_3}^+ + 3\,\mathrm{e}^- \tag{1}$$

and cathodic reduction by H_2 evolution and oxygen reduction at intermetallic cathodes outside the pit

$$6\,\mathrm{H}^+ + 6\,\mathrm{e}^- \longrightarrow 3\,\mathrm{H_2} \tag{2}$$

$$\frac{3}{2}\,\mathrm{O_2} + 3\,\mathrm{H_2O} + 6\,\mathrm{e}^- \longrightarrow 6\,\mathrm{OH}^-. \tag{3}$$

The overall pitting corrosion reaction of aluminum is

$$\mathrm{Al} + 3\,\mathrm{H_2O} \longrightarrow \mathrm{Al(OH)_3} + \frac{3}{2}\,\mathrm{H_2} \tag{4}$$

where insoluble aluminum hydroxide $Al(OH)_3$ and H_2 are formed [6]. Besides the pure detectability of atmospheric corrosion with today's AE measurement equipment, the present investigation also discusses the sources that generate AE signals. In particular, the question is addressed whether H_2 bubble activity is the only source or whether there are other effects that lead to AE signals. Therefore, two experiments on aluminum alloy AA2024-T351 specimens are conducted. The first experiment is designed to imitate atmospheric corrosion by local initiation followed by dry and wet phases, as it could be also expected during

 doi:10.20944/preprints202208.0097.v1

the operation of an aircraft. The second experiment is designed to confirm corrosion as the dominant source of AE signals. The corrosion is induced by small droplets of a 50 g/l sodium chloride (NaCl) solution of pH value 3. During both experiments, AE signals are permanently acquired. Furthermore, the region of the applied droplet is visually observed by video recording during all important phases of the atmospheric corrosion experiment. The atmospheric corrosion of an operating aircraft is simulated by a controlled variation of the ambient RH at room temperature after the application of the droplet. The correlation of H_2 bubble formation, AE hits and RH is analyzed.

2. Experimental Investigation

2.1. Specimen Preparation

Raw material for the investigation was a 1.6 mm thick plate of aluminum alloy AA2024-T351 with protective aluminum cladding (99.5 % purity) layers on both plate sides. The Al-cladding was removed by pickling the plate in a 10 % sodium hydroxide solution at 50 °C to 60 °C for about 10 min which results in a thickness reduction of about 0.2 mm. Subsequently, three specimens of dimension 40 mm × 28 mm × 1.4 mm were cut out of the pickled plate. Circular piezoelectric wafer active sensors (PWAS) of dimension Ø10 mm × 0.5 mm and material type Pi Ceramic PIC151 were applied to the center of the specimens as sensing elements for AE monitoring. Before the PWAS were adhesively bonded the corresponding surface area on the specimen was slightly ground and cleaned with a commercially available universal cleaner. Finally, the sensors were electrically contacted with shielded cables. Figure 2 shows a fully prepared specimen.

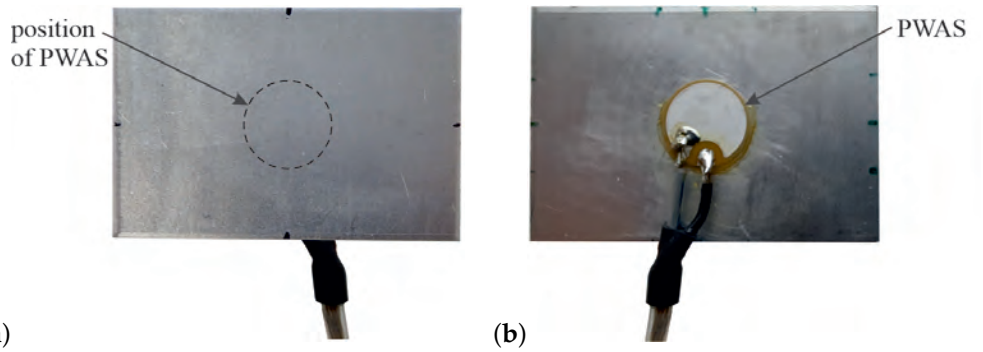

Figure 2. Aluminum specimen with applied and contacted PWAS (**a**) top side and (**b**) bottom side with applied and contacted PWAS.

2.2. Acoustic Emission Monitoring

The AE method is a passive SHM method, i.e., no actuators are used for excitation of the structure. The AE method evaluates transient elastic waves triggered by the time-discrete introduction or release of mechanical energy. The introduction of energy can result from, e.g., turbulence of a surrounding medium. However, AE is mostly referred to the sudden release of elastic energy, e.g., due to crack propagation. For the latter, already existing damages like a non-growing crack or non-active corrosion cannot be detected [28,29].

AE testing has a long history in NDT applications for temporary investigation of structures, thus, such commercially available sensors are often bulky and applied to and removed from many different structures. However, the sensing element of such sensors is typically a piezoelectric transducer [28]. In a SHM concept sensors should ideally be small, lightweight and unobtrusive or even integrated into the structure. Furthermore, sensors are attached permanently and need not to be removed after a testing routine like it is typically done in NDT. Thus, the use of PWASs for AE monitoring of structural damages as described in the section above, is a suitable approach [29–32].

 doi:10.20944/preprints202208.0097.v1

2.3. Atmospheric Corrosion Experiment – Setup and Procedure

This experiment represents a comprehensive study of atmospheric corrosion on an AA2024 alloy plate. It is conceptualized to simulate operational environmental conditions of an aircraft that promote corrosion. The experiment shall demonstrate the applicability of AE to atmospheric corrosion monitoring of aluminum aircraft components by today's measurement equipment. Furthermore, it is intended to investigate the dependency of corrosion on the ambient RH. Visual inspection of the corroding surface is implemented to correlate the ambient RH and the AE activity with the propagation of the corrosion.

Atmospheric corrosion is induced by a small droplet of a corrosive 50 g/l NaCl solution of pH 3 (glacial acetic acid added). The highest sensitivity of the sensor is given when the corrosion site is as close as possible to the PWAS. Therefore, the droplet was placed in the center of the top side of the specimen, i.e., opposite to the PWAS, compare Figure 2.

The experimental setup is presented in Figure 3. It consisted of a closed cell with ambient air in which the RH was controlled and logged together with the temperature. This cell was built by a Petri dish of dimension Ø200 mm × 35 mm with a rubber sealing on the edge of the dish and placed on a rubber mat to obtain a tight cell, see Figure 3. Additionally, two clamps were used to press the Petri dish onto the rubber mat to further increase tightness (not shown in Figure 3 for visibility reasons). The specimen was supported on

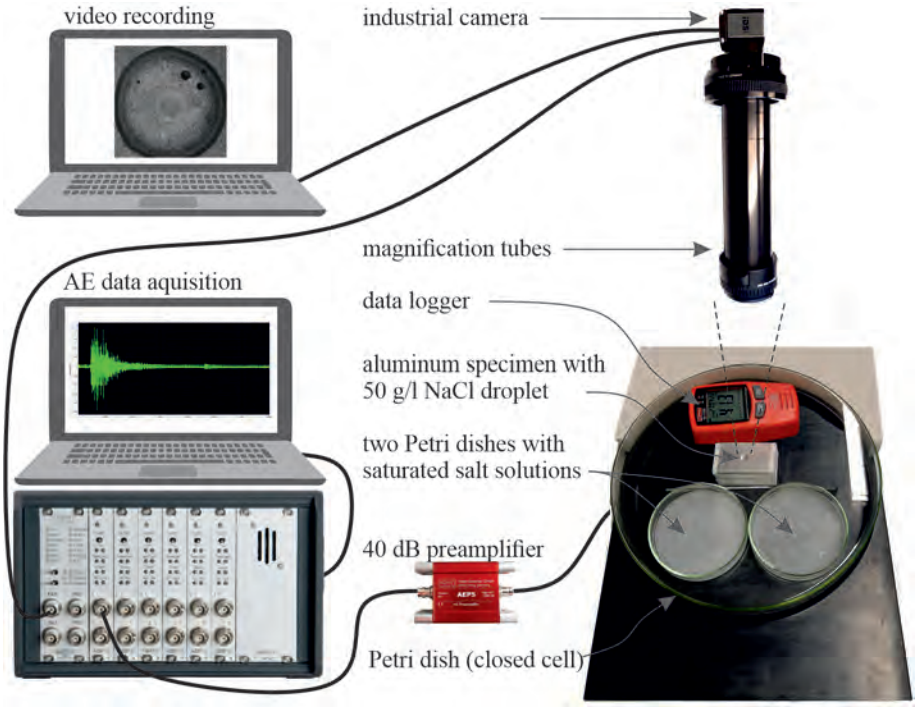

Figure 3. Experimental setup of the atmospheric corrosion experiment. AE monitoring of atmospheric corrosion during a controlled variation of the RH and additional visual observation of the corrosion by an industrial camera.

foam material placed inside the cell and was cleaned with acetone before the droplet was applied. The droplet was applied manually by a small syringe. Initially, a surface of 5 mm in diameter was wetted by the droplet with an approximate volume of 0.03 ml. The sensor cable was lead out through a tiny opening at the bottom of the rubber mat and connected via a preamplifier (type Vallen AEP5) with 40 dB amplification to the data acquisition (DAQ) system (type Vallen AMSY-6). The sampling rate was set to 20 MHz and the whole DAQ was controlled by an external notebook. The AE DAQ was done in continuous mode, i.e., a gapless AE data stream was recorded except for some time points described later. Consequently, the extraction of AE hits was done in post-processing by a defined amplitude threshold. Furthermore, no digital frequency filtering was applied during DAQ.

 doi:10.20944/preprints202208.0097.v1

The droplet on the specimen was observed visually using an industrial camera (type IDS UI-3370CP Rev. 2) which was positioned vertically above and outside the Petri dish a tripod. Extension tubes were mounted between the camera and the lens for magnification of the droplet, see Figure 3. The resolution of the video recording was 2048 px × 2048 px. The recording was done by video sequences of 20 min in duration and a framerate of 35 fps. The videos were recorded at selected times rather than continuously. A digital output from the camera was used to connect the internal flash signal, triggered at frame capture, to the AE DAQ system to enable synchronization between AE and video data in post-processing. The camera was connected to a second external PC which controlled the video recording.

The RH under the Petri dish was controlled with various saturated salt solutions, a method which is often used in laboratory experiments [33,34]. The used salts for the saturated solutions with the corresponding equilibrium RH at 20 °C and 25 °C are listed in Table 1. The experimental procedure and the variation of the RH, simulating potential

Table 1. Equilibrium relative humidity (RH) of the used saturated salt solutions at 20 °C and 25 °C for the controlled variation of the RH in the closed cell [34].

Salt	Formula	RH at 20 °C (%)	RH at 25 °C (%)
Magnesium chloride hexahydrate	$MgCl_2 \cdot 6\,H_2O$	33.0	32.5
Magnesium nitrate hexahydrate	$Mg(NO_3)_2 \cdot 6\,H_2O$	55.0	53.0
Sodium chloride	NaCl	76.0	75.5
Potassium chloride	KCl	85.0	85.0
Sodium sulfate decahydrate	$Na_2SO_4 \cdot 10\,H_2O$	93.0	93.0

operating conditions of an aircraft, in the closed cell were as follows. The experiment started with the application of the droplet. The controlled variation of the RH was done by adding or exchanging two small Petri dishes containing the saturated solutions in a predefined sequence shown in Table 2. For the exchanges of the saturated solutions the big Petri dish (cover) was just opened as little and short as necessary, to affect the prevailing environment inside as less as possible. At the very beginning of the experiment high RH was used to avoid evaporation of the applied droplet on the specimen (step 1). After that, a slow decrease to low RH followed to induce gradual evaporation of the droplet (steps 1-5). This low RH was held until the droplet evaporated and the specimen was completely dry (step 5). Then the RH was slowly increased back to high values to force rewetting by deliquescence of the NaCl crystals left after the water evaporated from the droplet (steps 6-10). This rewetting only occurred at the NaCl crystals, no wetting was observed elsewhere on the specimen. Finally, after high RH was reached again an abrupt decrease to very low RH was induced using silica gel instead of a saturated salt solution to dry out and preserve the corroded specimens (step 11). The small Petri dishes were exchanged when the RH approached and only slightly deviated from the expected equilibrium values presented in Table 2. These exchange procedures have been the only interruptions of the continuous AE DAQ. Videos were also not recorded during these phases. The temperature and RH prevailing in the closed cell were continuously (also during the exchange of the saturated salt solutions) recorded with a data logger (type RS PRO RS-172TK).

2.4. AE Source Identification Experiment – Setup and Procedure

The purpose of this experiment is to investigate whether the measured AE signals from the atmospheric corrosion experiment and the resulting findings are truly related to corrosion, or whether other effects produce AE signals. Therefore, the difference in AE caused by a droplet of pure water and a droplet of the corrosive NaCl solution on two equal specimens within the same environment is analyzed.

Preprints (www.preprints.org) | NOT PEER-REVIEWED | Posted: 4 August 2022 doi:10.20944/preprints202208.0097.v1

Table 2. Sequence of used saturated solutions to control the RH in the closed cell.

Step	Solution Petri dish 1	Solution Petri dish 2	Expected RH (%)	Remark
0	-	-	-	ambient RH
1	$Na_2SO_4 \cdot 10\,H_2O$	$Na_2SO_4 \cdot 10\,H_2O$	93.0	initial high RH
2	NaCl	NaCl	76.0	start of drying
3	NaCl	$Mg(NO_3)_2 \cdot 6\,H_2O$	65.5	-
4	$Mg(NO_3)_2 \cdot 6\,H_2O$	$Mg(NO_3)_2 \cdot 6\,H_2O$	55.0	-
5	$MgCl_2 \cdot 6\,H_2O$	$MgCl_2 \cdot 6\,H_2O$	33.0	-
6	$Mg(NO_3)_2 \cdot 6\,H_2O$	$Mg(NO_3)_2 \cdot 6\,H_2O$	55.0	start of rewetting
7	NaCl	NaCl	76.0	-
8	KCl	-	85.0	-
9	$Na_2SO_4 \cdot 10\,H_2O$	-	93.0	-
10	H_2O	H_2O	>93.0	deionized water
11	silica gel	silica gel	<33.0	final drying

The experimental setup was similar to the one explained in Section 2.3 and is shown in Figure 4. The first specimen was applied with a droplet of Milli-Q water (water of highest purity) and the second specimen with a droplet of the 50 g/l NaCl solution. Each droplet initially wetted a surface of 9 mm in diameter and had a volume of approximately 0.1 ml. The two specimens each supported on foam material were put under the Petri dish, to create a closed cell, where both specimens were exposed to the same environmental conditions. High RH was controlled by two small dishes of saturated potassium chloride (KCl) solutions with a theoretical equilibrium RH of 85 % at room temperature, see Table 1, to prevent evaporation of the droplets. After about 8.7 h, enough data was believed to be acquired to draw reliable conclusions (based on previous tests), and the RH was rapidly decreased by exchanging the saturated KCl solution with silica gel. The experiment was ended after complete evaporation of the droplets was visually observed so that dry specimens were obtained. The sensor cables of both PWAS were lead out through a tiny hole at the bottom of the rubber mat and connected via preamplifiers (type Vallen AEP5) with 40 dB amplification to the DAQ system (type Vallen AMSY-6). The same measurement equipment as for the atmospheric corrosion experiment was used. In addition, the same DAQ settings as for the atmospheric corrosion experiment were used, except for the sampling rate which was 10 MHz for this experiment (the atmospheric corrosion experiment suggested this sample rate to be sufficiently high). The DAQ was controlled by an external notebook. The temperature and RH inside the cell were measured with a data logger (type RS PRO RS-172TK). In contrast to the atmospheric corrosion experiment, no visual observation by video recording was conducted.

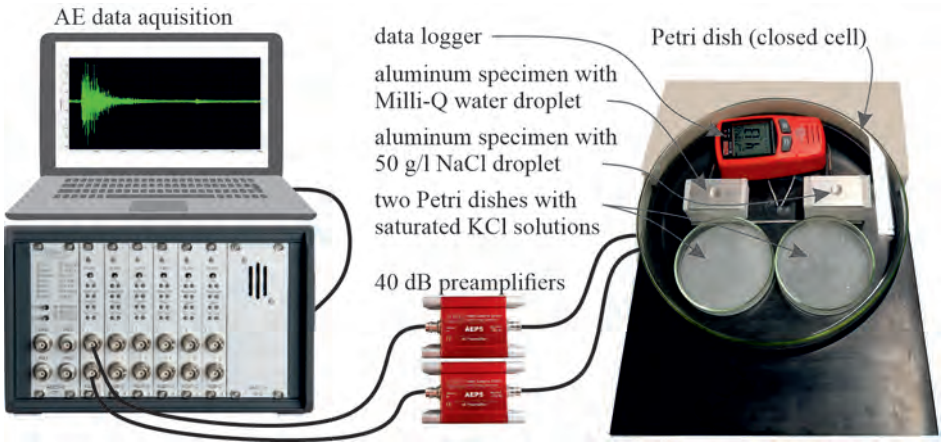

Figure 4. Experimental setup of the AE source identification experiment to compare AE due to droplets of Milli-Q water and the NaCl solution, respectively.

Preprints (www.preprints.org) | NOT PEER-REVIEWED | Posted: 4 August 2022 doi:10.20944/preprints202208.0097.v1

3. Results and Discussion

3.1. Comparison of AE, Bubble Activity and Atmospheric Corrosion

Figure 5 shows the curve of the measured RH and temperature T during the atmospheric corrosion experiment which lasted about 96 h. The temperature varied periodically with the day-night cycle, minimum values during night have been 22 °C and maximum values during day 25 °C. The time points of the exchanges of the saturated salt solutions, i.e., the change between the steps, can be seen clearly by the abrupt decreases or increases of the RH curve. Although the expected RH values, as given in Table 2, were not achieved for the saturated salt solutions used accordingly, the RH variation was suitable to simulate dry and wet phases at the monitored specimen, as expected in the operation of aircraft components. Moreover, Figure 5 shows several images of the specimen surface with the applied droplet (extracted from the recorded videos) and the corresponding time points. Figure 5a shows the droplet 2.8 h after the start of the experiment, where a high RH of 77 % was present. Bubbles of different sizes are clearly visible in the droplet. Due to the absence of other bubble-forming processes and corrosion taking place (as it can be seen later), this is H_2 produced by corrosion processes. Figure 5b shows the surface of the specimen at hour 23.5 which was the end of the defined decrease of the RH to 33 %. The steady decrease in RH caused the water to slowly evaporate from the specimen surface, while the NaCl crystals of the droplet solution remained on the surface. Furthermore, already clear pitting corrosion can be observed in that image. Figure 5c shows the surface at hour 54.9 at a RH of 79 %. Due to deliquescence, moisture of the humid environment was absorbed by the NaCl crystals which resulted in numerous smaller droplets of an again corrosive NaCl solution. Figure 5d depicts the situation at hour 74.6 and about 83 % RH which is only briefly before the maximum reached RH of 85 %. Due to increasing duration and RH, the droplets increased further in size and partly merged. Moreover, by comparison of Figures 5b-d the growth of readily existing pits and the formation of new pits can be clearly observed. Figure 5e shows a completely dried out but corroded surface after 95.8 h at a RH of 7 %. Significant pits and NaCl crystals can be identified. Minor pit growth between Figure 5d and Figure 5e is also expected, but due to the short time (about 2 hours) in which electrolyte is present on the specimen in this period, this is not visually apparent. After the rapid decrease in RH at hour 76.7, pit growth stops.

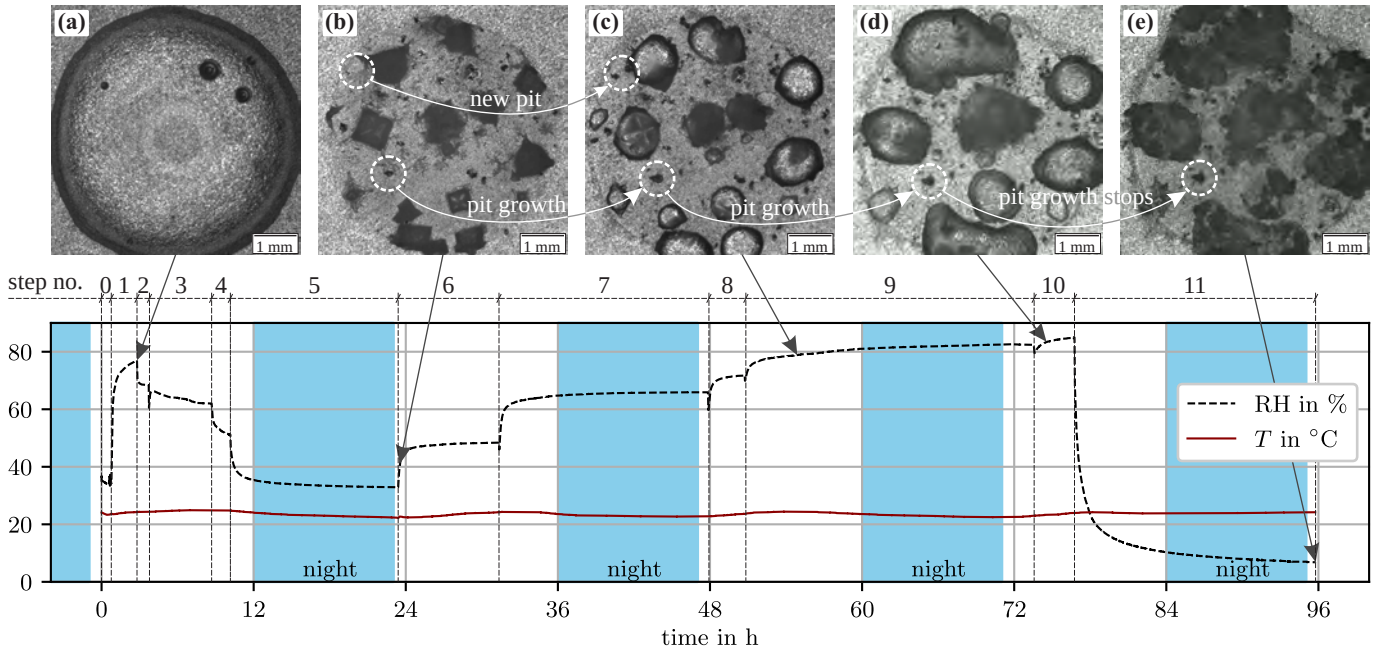

Figure 5. Relative humidity (RH) and temperature T during the atmospheric corrosion experiment and exemplary images **(a)** to **(e)** of the applied droplet and the corroded surface. The areas marked in blue represent the night times from 8 pm to 7 am.

Preprints (www.preprints.org) | NOT PEER-REVIEWED | Posted: 4 August 2022 doi:10.20944/preprints202208.0097.v1

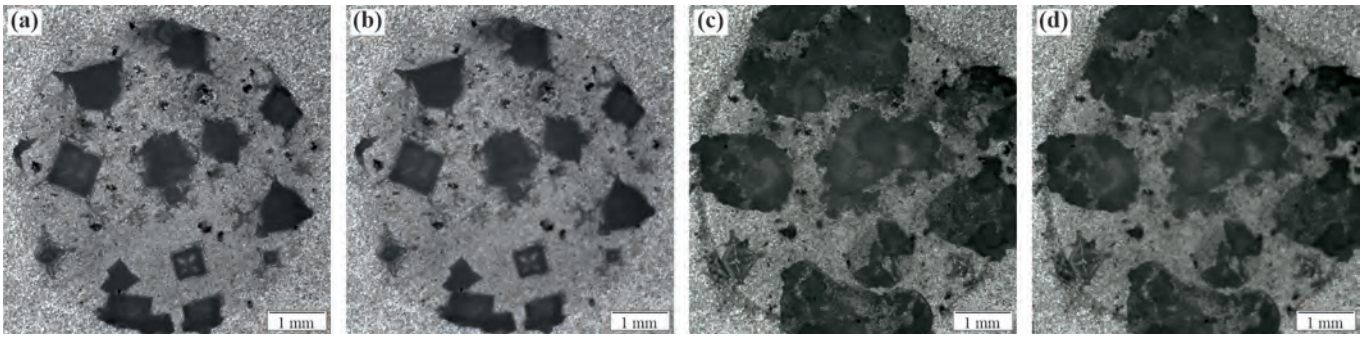

Figure 6. No progress of corrosion during the defined dry phase, i.e., no difference can be seen between the corroded specimen surfaces **(a)** at hour 23.5 and **(b)** at hour 27.5. No progress of corrosion after the final evaporation of the droplet as well, **(c)** shows the specimen surface at hour 77.7 and **(d)** at hour 95.8.

Figure 6 illustrates that corrosion did not progress during dry phases at low RH. Due to some issues with the video control, some lacks exist where no videos were recorded, e.g., in the dry phase from hour 9.8 to hour 23.5. Therefore, Figure 6a shows the specimen surface at hour 23.5, i.e., at the end of the defined dry phase, and Figure 6b the surface at hour 27.5 at a RH of 47 % where the specimen surface was also still dry. No pit growth or formation of new pits can be identified within this time span. However, a closer look at the corresponding videos, reveals single tiny bubble activity already started again at hour 27.5. Therefore, also the dry phase at the end of the experiment is analyzed. Figure 6c shows the dry specimen surface at hour 77.7 at a RH of 27 % and Figure 6d the surface at the end (18.1 h later) of the experiment, i.e., the same frame as in Figure 5e. No differences can be found between Figure 6c and d. Moreover, no bubble activity is observed in the videos recorded during the corresponding time period. Thus, it is concluded that corrosion did not progress during the two dry phases of the experiment.

To address the initial question of whether atmospheric corrosion can be measured with AE, and further, how it is related to the RH, the measured AE, video and RH data are processed and analyzed to determine if correlations exist. The AE activity is represented by a cumulative AE hit count. An amplitude threshold of 28 dB, with reference voltage $V_{\text{ref}} = 1\,\mu\text{V}$ [28], is used for the extraction of single hits out of the continuous AE data stream. The threshold is defined to be 3 dB above the noise level (proved to suppress small noise outliers), which is approximately constant at 25 dB for the entire AE data. Further, for all the detected hits a 5 ms time signal is used for further analysis, i.e., a predefined hit duration is applied. The 5 ms duration is enough to fully record most AE events that triggered a hit. Although the experiment was conducted under laboratory conditions electrical interference could not be completely avoided. However, such interference typically generates spike-like AE signals with high amplitude but only very little (often just single) counts (number of positive threshold crossings) [28,35]. These interferences are filtered out by not considering AE hits with less than five counts.

For the monitoring of the corrosion propagation, the videos are visually inspected (results are exemplarily presented in Figure 5 and Figure 6). It was observed, that the corrosion of aluminum and its constant production of H_2 also forms bubbles when there is only very little electrolyte present on the aluminum surface. These bubbles are reported to be one of the major sources of AE in immersion-like tests [23–25], thus, the observed small H_2 bubbles are believed to be also a major AE source in the present atmospheric corrosion experiment. To investigate this question, the recorded videos are processed using an algorithm implemented in Python 3.8 that automatically detects sudden changes like moving, merging or bursting bubbles. In a first step background subtraction, using the OpenCV package, is conducted to highlight sudden changes in the videos. In a second step event detection by evaluating the size of these changes using the imutils and the OpenCV Python package is performed. In cases when the detected events exceed a certain threshold

Preprints (www.preprints.org) | NOT PEER-REVIEWED | Posted: 4 August 2022 doi:10.20944/preprints202208.0097.v1

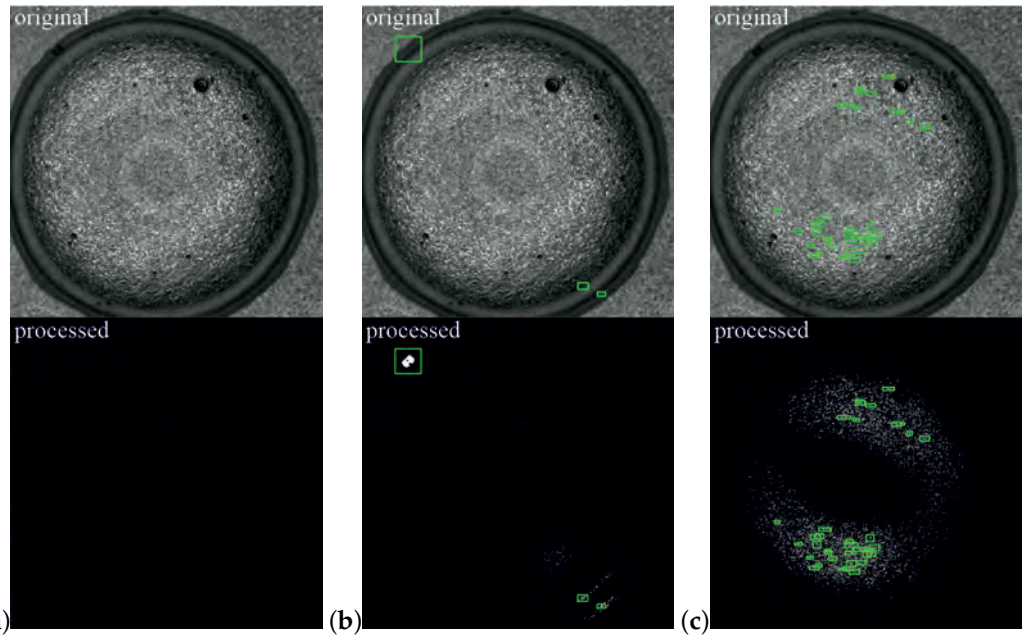

(a) (b) (c)

Figure 7. Example results of the video processing algorithm. The upper part of the images represents original captured frames and the lower part processed frames. (**a**) Bubbles in the droplet can be seen in the original frame but the algorithm detects no activity, (**b**) shows the subsequent frame. The bubble at the upper left edge of the droplet has burst, which is detected by the algorithm and highlighted with a green rectangle. (**c**) A small vibration in the video caused 37 detections at once, such disturbances are not considered in the further analysis.

size, the events are considered to be relevant. For comparison with the AE data processing a cumulative count of the detected events over time is generated. Figure 7 shows some exemplary results of a processed video recorded in step 1. The upper part of the images shows an originally captured frame and the lower part shows the corresponding processed frame. The original frame in Figure 7a shows several bubbles in the droplet, but only very little changes from the previous frame were detected, resulting in an almost black processed frame. Figure 7b shows the subsequent frame. The bubble at the upper left edge of the droplet has burst, which is detected by the algorithm and highlighted with a green rectangle. Additionally, two smaller events are detected in the lower right corner of the frame. A threshold size of 60 pixel was decided by the authors to be a proper value to avoid invalid detection of noise or other artificial objects caused by little vibrations or shocks of the setup. However, larger shocks of the setup caused several detections at the same time, which result in a heavily disturbed cumulative count, compare Figure 7c. Such disturbances are removed from the cumulative count in a final processing step. Manual inspection of some processed videos reveals that there is predominantly H_2 bubble activity in the videos and that this activity is well captured by the video processing algorithm. Furthermore, manual inspection reveals, that in most cases a maximum of three to four valid objects are detected between two consecutive frames. Thus, if five or more objects are detected simultaneously, the corresponding counts are removed. In another cleaning step, a check is made to see if an event was detected at the same or a nearby position in the previous frame, thus, avoiding the multiple counting of single events of larger duration (e.g., slow movement or rise of a bubble).

The generated cumulative counts of the AE and video data are shown together with the curve of the RH in Figure 8. As already mentioned above, there are some lacks where no videos were recorded, especially in the time span from hour 10.6 to hour 23.5, which is illustrated by the solid line without the markers at the curve of the cumulative video event count in Figure 8. Figure 8 clearly shows that the cumulative AE hit count and the cumulative video event count are related to the RH, or more precisely, to the resulting

Preprints (www.preprints.org) | NOT PEER-REVIEWED | Posted: 4 August 2022 doi:10.20944/preprints202208.0097.v1

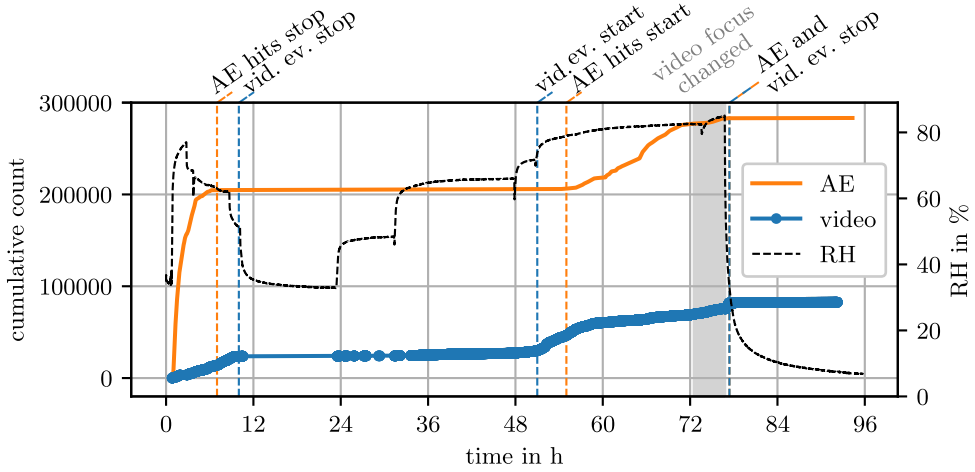

Figure 8. Measured relative humidity (RH) and calculated cumulative counts of AE and video data of the atmospheric corrosion experiment. The vertical dashed lines represent the times when the cumulative counts of AE and video data indicate a stop and start of corrosion activity. The gray area marks a time span in which the focus of the camera was changed.

presence of electrolyte on the specimen surface. In the initial phase, when the RH rises steeply to high values so that the droplet of the NaCl solution remains on the specimen and does not evaporate, both cumulative counts show a significant increase. After about 3.7 h and a RH drop to 66 %, which is after the second exchange of the saturated salt solutions, the curve of the cumulative AE hit count significantly flattens. The corresponding videos show that some water of the droplet has already evaporated, thus, less solution is present on the specimen. After about 7 h at a RH of 63 % stagnation of this curve can be observed, while the curve of the cumulative video event count starts to stagnate later, after about 9.8 h at a RH of 51 %, which is around the third exchange of the saturated salt solutions. Although there is a lack of videos as explained above, the described stagnation of the cumulative video event count is considered to be valid, as the curve flattens significantly and remains constant at a very low level between hour 9.8 and hour 10.6. The corresponding video of the onset of the stagnation of the cumulative AE hit count shows that the water of the droplet has already evaporated, moreover, small pits have formed on the corresponding specimen surface. However, although the surface of the specimen seems to be dry, small bubbling can be still observed, which are also detected by the video processing algorithm. This bubbling takes place in and in the near vicinity of already existing and emerging pits. These observation demonstrates that a seemingly dried out surface does not mean that corrosion is no longer taking place. If the surface is already partially corroded in the form of pitting, electrolyte can remain in pits and allow corrosion to progress further. This is expected due to two reasons, (i) the drying of the pits simply takes longer as, e.g., corrosion products around the pits build a barrier to the environment, or (ii) due to deposits and surface conditions of the specimen the equilibrium RH is reduced inside the pits [6]. At hour 23.5 where the RH reaches its preliminary minimum of 33 % and it is started to force the RH to rise again, the corresponding video shows a dry specimen and no more bubbles can be seen in the pits, compare Figure 5b. About 20 min after that at a RH of about 44 %, again first small bubbling at pits can be observed, which leads to a slightly progressive increase of the cumulative video event count until hour 51 where RH increases to about 74 %. At this point, small droplets can be clearly seen on the surface of the specimen. In addition, the large NaCl crystals begin to deliquesce due to the high RH that is very close to its equilibrium or deliquescence relative humidity (DRH), compare Table 1. From the point where the NaCl crystals start to deliquesce, and thus, become a liquid solution again, see Figure 5c, the curve of the cumulative video event count increases again significantly, as the liquid electrolyte promotes the corrosion, thus, more and probably larger bubbles are formed that are detected by the video processing algorithm. The progress of corrosion can

 doi:10.20944/preprints202208.0097.v1

further be observed by the increasing size of several pits, compare Figure 5b-d. The curve of the cumulative AE hit count starts to increase again at hour 55 at a RH of 79 %. Final and maximum RH is about 85 % and it is reached at hour 76.7. Thereafter, the RH is rapidly decreased to a low level by the use of silica gel. After further 40 min the cumulative AE hit count clearly stops to increase. The same holds for the cumulative video event count. Also about 40 min after the RH reduction stagnation of the cumulative video event count is observed. Thus, due to the rapid reduction in RH, AE and video activity stop rather simultaneously, i.e., electrolyte in the pits also evaporates rapidly. These findings clearly confirm that corrosion took place during the period of significant AE and bubble activity and vice versa.

The curve of the cumulative AE hits shows its steepest increase at the beginning and clearly flattens after 3.7 h. At hour 55 the curve starts to increase with a slope similar to that between hour 4 and hour 7, i.e., during the evaporation of the droplet before. These similar slopes seem plausible since similar conditions prevail at these times (similar amount of highly concentrated electrolyte at similar locations). Thereafter, the curve increases gradually but remains constant on average until the forced drying at hour 76.7. This trend shows clearly that most AE hits are detected at the beginning of the corrosion and suggests a correlation of AE hits to the amount of electrolyte present on the specimen.

The slope of the cumulative video event count in the time span at the beginning (hour 0 to hour 10) and at the start of the deliquescence of the NaCl crystals (hour 51 to hour 59) is similar. In the first time span, the focal plane of the camera was set near the droplet surface where bubbles in the droplet are clearly visible. In the second time span, the focal plane was set at the specimen surface where the small bubbles in and near the pits are observed. From hour 59 on, more and more electrolyte in the form of single droplets is present on the specimen due to ongoing deliquescence of the NaCl crystals. However, due to the focal plane settings of the camera bubbles appear blurred in the droplets of electrolyte and are less well detected by the algorithm. This is considered to be the reason for the flattening of the cumulative video event count curve between hour 59 and hour 72.5. From hour 72.5 to hour 76 the setting for the focal plane is changed, see the gray marked area in Figure 8. The focal plane was moved slightly above the specimen surface. This modification made bubbles partly visible. However, blurred bubbles are still present at the edges of the droplets, which are not detected by the algorithm. Thus, if there are several small droplets on the specimen, only a portion of the bubbles within these droplets can be detected, i.e., changing the focal plane does not significantly change the trend of the cumulative video event count, compare Figure 8.

From a global perspective, both cumulative curves show similar trends that are both related to the measured RH. A stopping of corrosion when RH comes to low values is observed in the videos (no pit growth or formation of new pits) and reflected in the cumulative video event count (no bubble activity). Also a re-onset of corrosion when RH is increased again is visually observed clearly. It is shown that such stops and restarts of atmospheric corrosion can also be detected with the AE method, however, with some time delay with respect to RH and bubble activity. It is observed that in the phases where just a little amount of solution is present on the specimen or only in pits, also less and smaller bubbles are formed. It is expected that these small bubbles are too weak to generate AE events that exceed the noise level, and thus, are not detected by the simple amplitude threshold approach used. The visual observation by the videos strongly suggests bubbles to be the main source for the measured AE signals, as only very few events different from bubbles were observed or detected. Such other events detected have been, e.g., little but sudden growth of the small droplets during rewetting or merging of these droplets during rewetting, but also sudden shrinkage of the droplets during the phase of the rapid RH reduction at the end of the experiment. Besides the presented comparison of cumulative counts from video and AE data also a specific assignment of bubble activity to AE hits and vice versa was attempted. Therefore synchronization of the corresponding two timelines was required which was enabled by the flash signal of the camera (triggered at each video

Preprints (www.preprints.org) | NOT PEER-REVIEWED | Posted: 4 August 2022 doi:10.20944/preprints202208.0097.v1

frame) that was connected to a parameter channel of the AE measurement system, see Figure 3. However, no clear assignment could be found. The reasons therefore are expected to be the lack of depth of field, a too low video framerate of 35 fps, i.e., a frame interval of approximately 29 ms compared to a typical AE hit duration of 5 ms and the unclear effects of the bubbles (formation, detachment, movement, arrival at droplet surface, growth, bursting) that actually generate the AE event.

3.2. Frequency Analysis of Atmospheric Corrosion AE Data

The frequency analysis of the AE data of the atmospheric corrosion experiment shall identify further AE activity that is not detected by the simple amplitude threshold approach. However, due to the very large amount of AE data, a meaningful visual representation of time-frequency domain analysis results is challenging. Thus, a frequency analysis, based on the short time Fourier transform (STFT), of the complete AE data is conducted, but only dominant frequencies are plotted. Therefore, the entire AE dataset is divided into n_{seg} segments each of 0.1 s duration, which are transformed into the time-frequency domain by the STFT. For each transformation result $Z_i(f,t)$ the frequency $\hat{f}_i$ of the maximum of the absolute value of $Z_i(f,t)$, i.e.,

$$\hat{f}_i = \arg\max_f \operatorname{abs}(Z_i(f,t)) \tag{5}$$

with $i = 1 \ldots n_{\text{seg}}$ is extracted. The STFT is calculated using the command signal.stft of the Python package scipy. The Hann window with a window length of $w = 2500$ samples and a window overlap of $w/2$ is used, leading to a time resolution of 62.5 µs and a frequency resolution of 8 kHz. Figure 9 shows the result of this frequency analysis together with the curve of the RH.

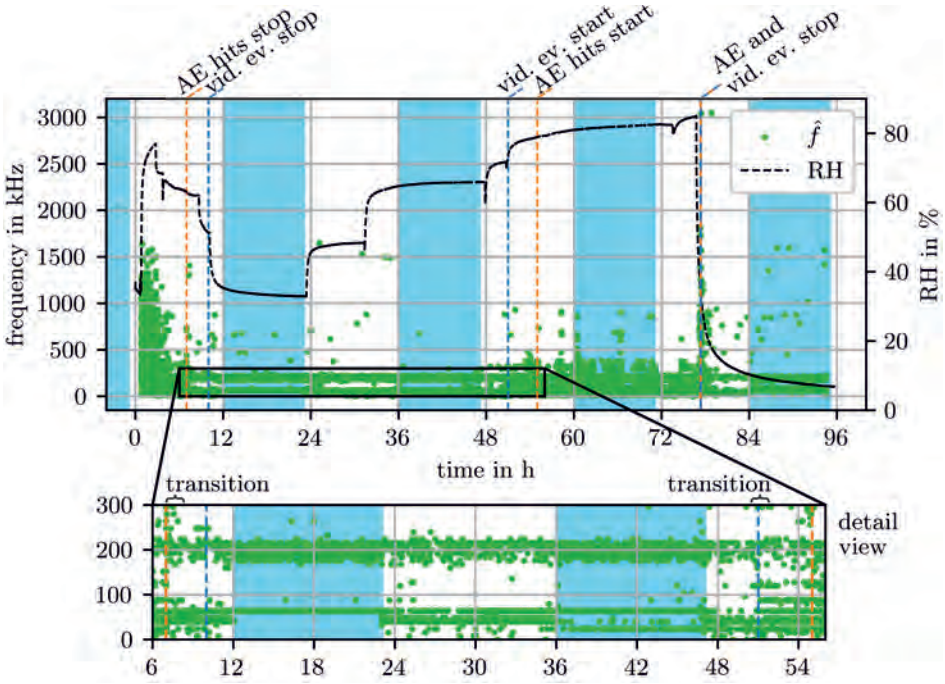

Figure 9. RH and result of the STFT-based frequency analysis of the entire AE data of the atmospheric corrosion experiment. The colored vertical dashed lines represent the times at which the cumulative AE hits and the cumulative video event count indicate the stop and the start of corrosion activity. The areas marked in blue represent the night times from 8 pm to 7 am. The detail view highlights the different frequencies at day and night times, as well as the transitions between frequencies indicating corrosion activity and constant frequencies due to background noise.

 doi:10.20944/preprints202208.0097.v1

Clear differences in the calculated frequencies between wet and dry phases, i.e., phases of high and low RH, can be seen. Especially, in the beginning when the initially applied droplet is present on the specimen, frequencies up to 1.5 MHz are yielded. The reduction of RH, and thus, electrolyte on the specimen surface, results also in a reduction of the frequency. Between hour 12 and hour 48, always the same frequencies are determined. In this time span, low RH prevails and the NaCl crystals have not started to deliquesce yet. A detailed analysis of these frequencies (by the experimental measurement of the electromechanical impedance spectrum of the specimen with applied PWAS), reveals that some of them fit to natural frequencies of the specimen. Moreover, it is observed that day (7 am to 8 pm) and night times (8 pm to 7 am) influence these frequencies clearly, compare detail view in Figure 9. This influence has to be considered when attempting to determine the transition from frequencies indicative of corrosion activity to frequencies due to background noise. The transition indicating the stop of corrosion due to lowering the RH is suggested to be approximately at hour 7.5, which is between the stopping points determined by the cumulative AE hits and the cumulative video event count. The onset of corrosion activity due to the increase of the RH is determined to be approximately at hour 51.2, which matches with the point of the cumulative video event count.

The frequency behavior after hour 51.2 is again clearly different from the phase with low RH before. However, the maximum reached frequencies are lower than in the initial phase where the full droplet is present on the specimen. The rapid reduction of RH at the end of the experiment leads to a short but significant increase of frequencies with peak values of nearly 2 MHz. A detailed view of this result reveals, that this happens about 30 min after the start of drying out at a RH of 37 % and ends about 12 min later, i.e., this fits well to the end of the increases of the cumulative counts above. The corresponding videos show, that at the beginning of this time span the specimen surface is already dry, but the remaining NaCl still is slightly soaked with some water. In the following 10 min, the last of the water evaporates, leaving dry NaCl deposits on the specimen surface, as can be seen in Figure 5e. Thus, this high frequency AE activity may be also from other sources than corrosion, e.g., the very fast drying of the surface and its deposits. However, due to the very short duration of these possibly disturbing additional AE sources, effects on the experimental findings of the cumulative hit count can be excluded.

The frequency analysis shows that further information can be extracted from the AE data. The low bubble activity in the pits could not be fully detected with this frequency domain analysis. However, the transitions of the dominant frequency activities assigned to corrosion to frequencies of background noise and vice versa shift towards the corresponding observation points of the cumulative video event count.

3.3. AE Evaluation of AE Source Identification Experiment

The AE data of the AE source identification experiment is evaluated by the cumulative AE hit counts of both AE datasets (specimen subjected to Milli-Q water droplet and specimen subjected to NaCl solution droplet). A threshold value of 25 dB is used for hit extraction. The threshold is defined to be 3 dB above the noise level (prooved to suppress small noise ouliers), which is approximately constant at 22 dB for both AE data streams. Furthermore, for all the detected hits a 5 ms time signal is used, i.e., a predefined hit duration is applied. The 5 ms duration is enough to fully record most AE events that triggered a hit. Figure 10 shows the cumulative AE hit counts due to the droplet of Milli-Q water and due to the droplet of the NaCl solution, as well as the curve of the measured RH in the closed cell. The start value of the RH is 38 %, which was the ambient RH before the setup was closed. Due to the saturated KCl solution, a steep increase of the RH follows which is intended to avoid evaporation of the droplets. After 2.1 h the equilibrium RH of NaCl (75.5 %) is reached and a final RH of about 80 % is generated after 8.7 h. After that period of high RH, evaporation of the droplets is forced by the use of silica gel, the experiment ends after 10.8 h with a steep decrease of the RH to 28 %. The temperature

Preprints (www.preprints.org) | NOT PEER-REVIEWED | Posted: 4 August 2022 doi:10.20944/preprints202208.0097.v1

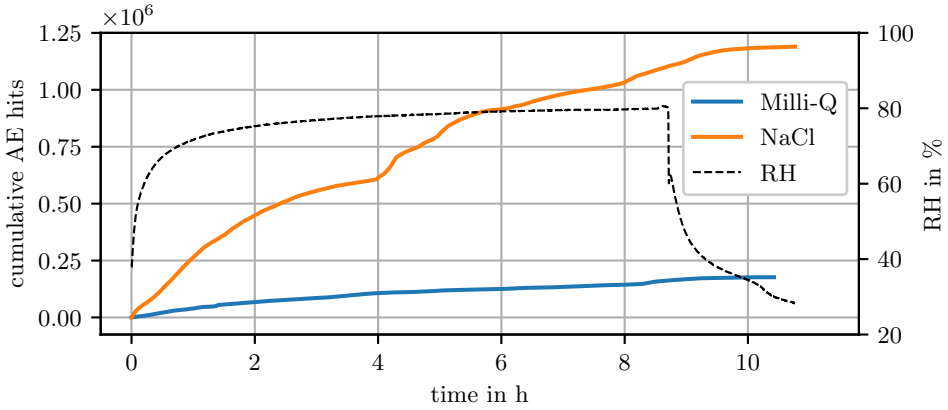

Figure 10. Relative humidity (RH) and cumulative AE hits caused by the droplet of Milli-Q water and the droplet of the NaCl solution, respectively, during the AE source identification experiment.

measured by the data logger, is nearly constant and varies between 23.6 °C and 25.1 °C with a mean value of 24.1 °C.

As already shown by the atmospheric corrosion experiment, the droplet of the NaCl solution generates a significant number of AE hits. The corresponding curve of the cumulative AE hits in Figure 10 shows a stronger increase at the beginning followed by a kind of stepwise but on average constant trend between hours 2 and 9. With a delay of approximately 1 h after the evaporation of the droplets is initiated, the AE hits decrease and the last hit is detected after 10.8 h from the beginning of the experiment.

Interestingly, also the droplet of the Milli-Q water generates a not negligible number of AE hits. The corresponding curve of cumulative AE hits in Figure 10 shows a stronger increase at the beginning, followed by a more flat and stepwise trend between hours 2 and 9, i.e., qualitatively similar to the curve of the NaCl solution. The delay from evaporation initiation to the beginning of the flattening of the curve is about 45 min and the last hit is detected after 10.4 h. The difference in the cumulative AE hit counts after the Milli-Q water droplet evaporated, is a factor of 6.7. Although this is a big difference, Milli-Q water was not expected to produce a significant number of AE hits, as Milli-Q water was not expected to corrode the aluminum specimen. Thus, the question remains open whether the effect that triggers AE activity is related to corrosion or not.

For further examination, the areas of the specimens that were initially wetted with the droplets are analyzed using optical microscopy (type Olympus SZX10 with DP26-CU camera). Figure 11a shows the corresponding surface caused by the NaCl solution droplet. NaCl crystals that remained after evaporation of the water of the solution can be seen clearly. Moreover, some pits, indicating that corrosion happened, can be identified on the microscopic image, e.g., the detail view shows a pit of approximate size 115 µm × 135 µm. Figure 11b shows the corresponding surface caused by the droplet of Milli-Q water. The microscopic image indicates that also due to the Milli-Q water corrosion took place. This is concluded as (i) seemingly small pits can be observed, see the detail in Figure 11b with a pit of approximate size 50 µm × 60 µm, (ii) some distinct discolorations can be seen over a wide area, possibly due to a uniform type of corrosion and (iii) white depositions can be seen on the specimen, which is most likely aluminum hydroxide $Al(OH)_3$ formed during corrosion, compare Figure 1 and Equation 4.

3.4. AE Signal Source Discussion

The discussion of the true source of the AE signals is challenging based on the presented results. However, analytical considerations allow to access this important question. Figure 12a presents a classification of all possible effects that might provoke AE activity during the experiments. It is shown that atmospheric corrosion can be triggered on AA2024-T351 by a small droplet of a corrosive NaCl solution, as the visual observation

 doi:10.20944/preprints202208.0097.v1

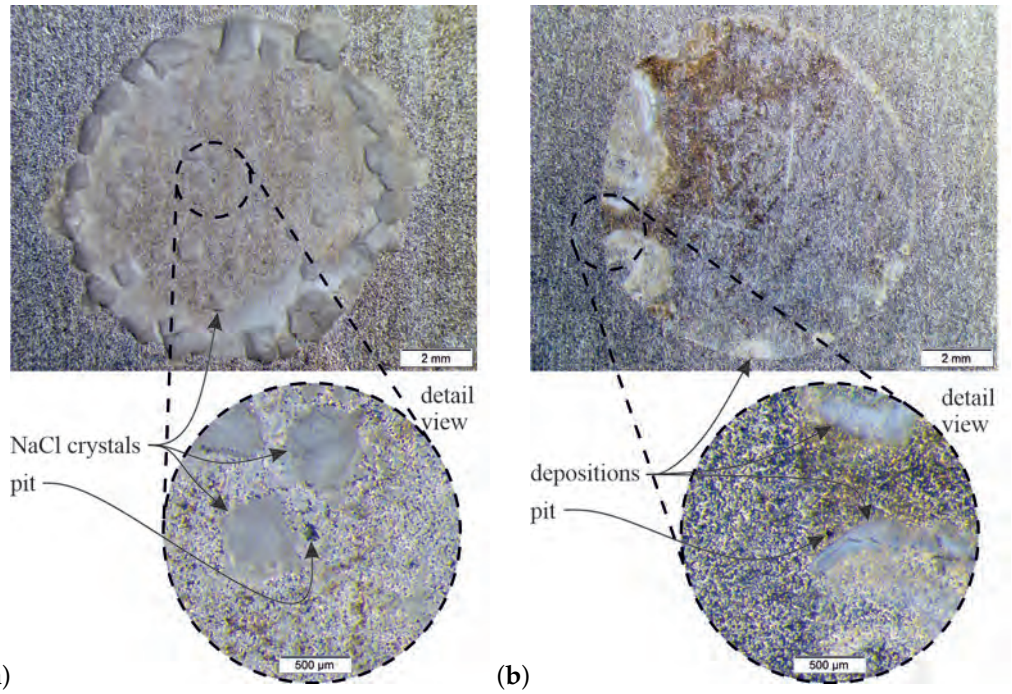

Figure 11. Microscopic images of the corroded specimen surface of the AE source identification experiment, i.e., after evaporation of the droplets of (**a**) the NaCl solution and (**b**) the Milli-Q water. The detail views show exemplary pits that were formed.

clearly identifies pits after some time. Hydrogen that is formed during corrosion leads to bubble activity which is also seen clearly in the videos and AE monitoring detects a significant number of AE hits. All three observed phenomena, i.e., corrosion, bubbles and AE hits, are associated with the RH, compare Figures 5 and 8, strongly suggesting that bubble activity (origination, detachment, movement, arrival at droplet surface, growth, bursting) is the main source for the measured AE signals, which is repeatedly claimed in literature for different kinds of corrosion tests [23–25]. However, it cannot be excluded that there are other unknown effects that generate measurable AE signals. Such other effects could be related to corrosion or not, compare Figure 12. Since it is attempted to answer the question of whether atmospheric corrosion can be clearly detected by AE, sources not related to corrosion should ideally be excluded or known. For the sole result of the specimen subjected to the NaCl solution no distinction between the named effects can be done. However, considering the second specimen, which was subjected to Milli-Q water, and thus, was less corroded, the AE activity (which was also less) can be directly assigned to be dominated by corrosion effects.

Figure 12b presents again the classification of all possible effects that might provoke AE activity during the experiments, but reduces the representation of the AE activity and its triggering effects that are suppressed by the use of Milli-Q water instead of the NaCl solution. Milli-Q water generates corrosion and also measurable AE signals. Compared to corrosion caused by the NaCl solution, corrosion caused by Milli-Q water is found to be significantly less. Less corrosion means less formation of H_2, compare Equation 4, i.e., less bubble activity and also less other effects that trigger AE activity related to corrosion. The cumulative AE hit count due to Milli-Q water is lower by a factor of 6.7 compared to the NaCl solution. Thus, it can be concluded that the measured AE hits are strongly dominated by corrosion-related effects. The insignificance of AE signals due to effects unrelated to corrosion can also be illustrated by the following considerations. Under the very conservative assumption, that the measured AE hits caused by Milli-Q water are only due to sources unrelated to corrosion and that these sources are assumed to occur at the same rate for the NaCl solution (same droplet sizes and equal environmental

Preprints (www.preprints.org) | NOT PEER-REVIEWED | Posted: 4 August 2022 doi:10.20944/preprints202208.0097.v1

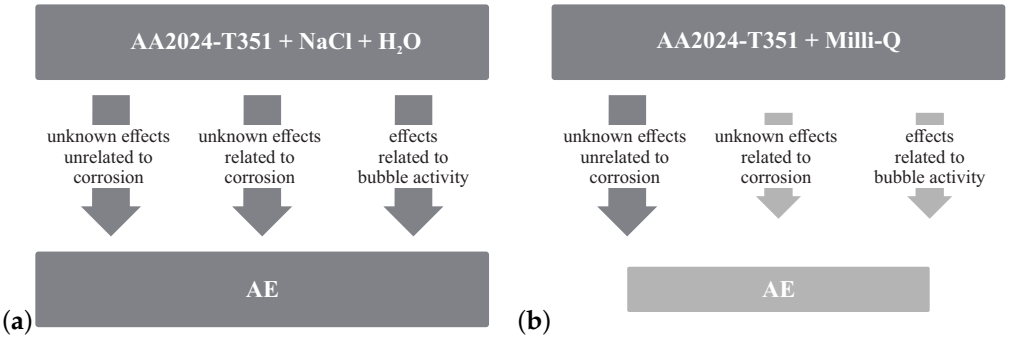

Figure 12. Classes of effects triggering AE activity on AA2024-T351, (**a**) corrosion and AE activity due to the NaCl solution and unknown contribution of different effect classes, (**b**) reduced corrosion and AE activity due to Milli-Q water, and consequently, reduced corrosion related effect class contributions.

conditions), corrosion-related sources occur 5.7 times more frequently than non-corrosion-related sources. However, the results above show that Milli-Q water also causes corrosion and that the measured AE hits are mainly driven by corrosion. Therefore, the factor between corrosion-related and non-corrosion-related sources has to be larger than 5.7. Consequently, non-corrosion-related effects cannot be fully excluded to contribute to the cumulative AE hit count but are shown to be of minor importance to the found results.

To identify valid AE sources, various potential effects are discussed and their plausibility to be an AE source is evaluated. First, sources unrelated to corrosion are discussed. Environmental noise and interferences were very little as the experiments were conducted under laboratory conditions. Nevertheless, electric interferences, which typically produce spike-like AE signals, are filtered out by not considering hits with counts smaller than five. AE sources caused by effects of the used saturated salt solutions and the silica gel can also be excluded, as the AE data did not show sudden changes due to the exchange of the salt solutions or the silica gel.

Second, AE sources related to corrosion but not directly to bubble activity are discussed. A possible AE source could be the initiation or growth of micro cracks (starting from pits) in the aluminum matrix caused by the formation of H_2 bubbles from individual H^+ ions or by residual stresses in the matrix. However, micro cracks can be excluded since it would also trigger measurable AE activity while small H_2 bubbles are observed (i.e., ongoing corrosion) only in some pits, compare Figure 8 hour 7 to hour 10, and hour 51 to hour 55. Moreover, no significant residual stresses are expected in the simple, small and thin specimens. A further effect triggering AE activity may be the dissolution into Al_3^+ ions in the pits, compare Figure 1. However, this is a continuous process on atomic level, i.e., low energy for AE, thus, it is also very unlikely to be a potential AE source.

And third, AE sources related specifically to bubble activity are discussed. As presented in Figure 1 the main phases of a bubble are its formation, detachment from the metal surface, movement, arrival at the droplet surface, growth and bursting. The sudden formation of gaseous H_2 from single solid state H^+ ions could potentially generate a pressure wave leading to AE. This can be excluded since no AE hits are detected during the low RH phase when no droplets are present but small bubbles (indicating ongoing corrosion) are observed in some pits, compare Figure 8 hour 7 to hour 10, and hour 51 to hour 55. Other potential sources are the detachment of bubbles from the specimen and subsequent bubble movement, arrival of bubbles at the electrolyte surface and bubble growth, e.g., by merging of bubbles and finally bursting of bubbles, compare Figure 1. All these effects must also occur when only little electrolyte is present in the pits, however, no AE hits are detected in this case, compare Figure 8 hour 7 to hour 10, and hour 51 to hour 55. Therefore, it is assumed that the amount of electrolyte at the corrosion site influences whether AE hits can be detected or not. From the recorded videos it is observed that more electrolyte, i.e., larger droplets, lead to larger bubbles which are expected to generate AE hits of larger amplitudes.

 doi:10.20944/preprints202208.0097.v1

Moreover, a larger amount of electrolyte might create a higher counter pressure against the bubbles, resulting in bubble activity of higher energy, i.e., AE hits of higher amplitude.

Thus, the results strongly suggest that bubble activity is the main source of the measured AE signals. Bubble bursting is assumed to be the most emissive source, but also merging of bubbles is expected to produce measurable AE signals. However, the amount of electrolyte present at the corrosion site has to be large enough to result in measurable AE signals. Thus, better measurement equipment or more advanced data analysis methods may have an impact on the results.

4. Conclusions

In the presented experimental investigation, atmospheric corrosion of AA2024-T351 aluminum alloy, commonly used for aircraft structures, is monitored by the AE method using a permanently attached PWAS transducer. The atmospheric corrosion is induced by small droplets of a corrosive 50 g/l NaCl solution on a specimen of dimension 40 mm $\times$ 28 mm $\times$ 1.4 mm. Operating environmental conditions of an aircraft are simulated by a controlled variation of the RH. In addition, videos of the corrosion site are recorded to allow visual assessment of the corrosion process.

Pitting corrosion due to the droplet of the NaCl solution is clearly observable. A corrosion stop is forced by decreasing the RH so that the water of the solution evaporates and consequently NaCl crystals remain on the specimen surface. A re-onset of corrosion is shown by a subsequent increase of the RH, which causes the NaCl crystals to deliquesce, i.e., form a corrosive solution that allows corrosion to progress again.

Numerous signals are detected during AE monitoring. Evaluation of the cumulative AE hits and STFT-based frequency analysis of the total AE data show a correlation between AE activity, the RH or the amount of electrolyte present on the specimen and the corrosion progress. This leads to the clear conclusion that atmospheric corrosion can be reliably detected with today's AE measurement equipment. The recorded videos are processed by an algorithm to automatically detect sudden events between consecutive video frames. This algorithm mostly detects bubbles of H_2, that are formed when aluminum reacts with aqueous solutions. Evaluation of the cumulative AE hits and the AE frequency analysis, the visual cumulative bubble count, the RH and the observed progress of corrosion strongly suggest that H_2 bubble activity is the predominant source for the measured AE hits. A finding that is also supported by literature. Other effects that are potentially unrelated to corrosion are investigated and discussed by an additional experiment comparing AE activity and corrosion due to the NaCl solution and due to Milli-Q water, under the same environmental conditions, respectively. Although AE sources unrelated to corrosion could not be excluded completely, it is shown that such sources are of minor importance to the found results. A detailed discussion of potential effects of bubble activity leading to AE signals is conducted. Bubble bursting is assumed to be the most relevant source, but also merging of bubbles is expected to produce measurable AE signals. However, the amount of electrolyte at the corrosion site has to be large enough for the AE measurement system to detect bubbles or corrosion at all. Better measurement equipment or more advanced data analysis methods may improve these results. Nevertheless, operational conditions of aluminum structures in aircrafts are strongly expected to periodically result in a sufficient amount of electrolyte to enable corrosion monitoring with the AE method.

Future research is planned to find characteristic features of the corrosion-related AE signals to enable identification of corrosion in noisy environments. Furthermore, further experiments shall be designed to identify the true effects that trigger corrosion-related AE activity, thereby enabling a better understanding of signal features. Future work shall also address the localization of corrosion-triggered AE signals in structural components by means of more than one PWAS and the evaluation of corrosion type and extent.

Author Contributions: Conceptualization, T.E. and C.K.; methodology, T.E. and C.K.; formal analysis, T.E.; investigation, T.E.; resources, T.E. and C.K.; writing—original draft preparation, T.E.; writing—review and editing, T.E., C.K. and M.S.; visualization, T.E.; project administration, C.K.;

funding acquisition, C.K. and M.S. All authors have read and agreed to the published version of the manuscript.

Funding: The research leading to these results has received funding from Take Off programme. Take Off is a Research, Technology and Innovation Funding Programme of the Republic of Austria, Ministry of Climate Action. The Austrian Research Promotion Agency (FFG) has been authorised for the programme management.

Data Availability Statement: The data presented in this study are available upon request from the corresponding author.

Conflicts of Interest: The authors declare no conflict of interest.

References

1. du Plessis, A. Studies on Atmospheric Corrosion Processes in AA2024. PhD thesis, University of Birmingham, 2015.
2. Li, L.; Chakik, M.; Prakash, R. A Review of Corrosion in Aircraft Structures and Graphene-Based Sensors for Advanced Corrosion Monitoring. *Sensors* **2021**, *21*, 2908. doi:10.3390/s21092908.
3. Civil Aviation Authority. Corrosion and Inspection of General Aviation Aircraft - CAP1570. Available online: https://publicapps.caa.co.uk/docs/33/CAP1570_Corrosion.pdf (accessed on 25 July 2022).
4. Galea, S.; Trueman, T.; Davidson, L.; Trathen, P.; Hinton, B.; Wilson, A.; Muster, T.; Cole, I.; Corrigan, P.; Price, D. Aircraft Structural Diagnostic and Prognostic Health Monitoring for Corrosion Prevention and Control. In *Encyclopaedia for Structural Health Monitoring*; Wiley, 2009.
5. Schindelholz, E.; Kelly, R.G. Wetting Phenomena and Time of Wetness in Atmospheric Corrosion: A Review. *Corrosion Reviews* **2012**, *30*, 135–170. doi:10.1515/corrrev-2012-0015.
6. Vargel, C., Ed. *Corrosion of Aluminium*, 2. ed.; Elsevier: Amsterdam, 2020. doi:10.1016/C2012-0-02741-X.
7. Federal Aviation Administration. AC 43-4B - Corrosion Control for Aircraft. Available online: https://www.faa.gov/documentLibrary/media/Advisory_Circular/AC_43-4B.pdf (accessed on 25 July 2022).
8. Obot, I.B.; Onyeachu, I.B.; Zeino, A.; Umoren, S.A. Electrochemical Noise (EN) Technique: Review of Recent Practical Applications to Corrosion Electrochemistry Research. *Journal of Adhesion Science and Technology* **2019**, *33*, 1453–1496. doi:10.1080/01694243.2019.1587224.
9. Ma, C.; Wang, Z.; Behnamian, Y.; Gao, Z.; Wu, Z.; Qin, Z.; Xia, D.H. Measuring Atmospheric Corrosion with Electrochemical Noise: A Review of Contemporary Methods. *Measurement* **2019**, *138*, 54–79. doi:10.1016/j.measurement.2019.02.027.
10. Davis, G.D.; Dacres, C.M.; Krebs, L. EIS-Based In-Situ Sensor for the Early Detection of Coatings Degradation and Substrate Corrosion. In Proceedings of the CORROSION 2000. OnePetro, 2000.
11. Annamdas, V.G.M. Review on Developments in Fiber Optical Sensors and Applications. *International Journal of Materials Engineering* **/26/2011**, *1*, 1–16.
12. Fan, L.; Bao, Y. Review of Fiber Optic Sensors for Corrosion Monitoring in Reinforced Concrete. *Cement and Concrete Composites* **2021**, *120*, 104029. doi:10.1016/j.cemconcomp.2021.104029.
13. McAdam, G.; Newman, P.J.; McKenzie, I.; Davis, C.; Hinton, B.R.W. Fiber Optic Sensors for Detection of Corrosion within Aircraft. *Structural Health Monitoring* **2005**, *4*, 47–56. doi:10.1177/1475921705049745.
14. Venancio, P.G.; Cottis, R.A.; Narayanaswamy, R.; Fernandes, J.C.S. Optical Sensors for Corrosion Detection in Airframes. *Sensors and Actuators B: Chemical* **2013**, *182*, 774–781. doi:10.1016/j.snb.2013.03.059.
15. Turcotte, J.; Rioux, P.; Lavoie, J.A. Comparison Corrosion Mapping Solutions Using Phased Array, Conventional UT and 3D Scanners. In Proceedings of the 19th World Conference on Non-Destructive Testing, 2016.
16. Zhao, X.; Gao, H.; Zhang, G.; Ayhan, B.; Yan, F.; Kwan, C.; Rose, J.L. Active Health Monitoring of an Aircraft Wing with Embedded Piezoelectric Sensor/Actuator Network: I. Defect Detection, Localization and Growth Monitoring. *Smart Materials and Structures* **2007**, *16*, 1208–1217. doi:10.1088/0964-1726/16/4/032.
17. Calabrese, L.; Proverbio, E. A Review on the Applications of Acoustic Emission Technique in the Study of Stress Corrosion Cracking. *Corrosion and Materials Degradation* **2021**, *2*, 1–30. doi:10.3390/cmd2010001.
18. Ono, K. Review on Structural Health Evaluation with Acoustic Emission. *Applied Sciences* **2018**, *8*, 958. doi:10.3390/app8060958.
19. Tscheliesnig, P.; Lackner, G.; Jagenbrein, A. Corrosion Detection by Means of Acoustic Emission (AE) Monitoring. In Proceedings of the 19th World Conference on Non-Destructive Testing, 2016.
20. Bi, H.; Li, H.; Zhang, W.; Wang, L.; Zhang, Q.; Cao, S.; Toku-Gyamerah, I. Evaluation of the Acoustic Emission Monitoring Method for Stress Corrosion Cracking on Aboveground Storage Tank Floor Steel. *International Journal of Pressure Vessels and Piping* **2020**, *179*, 104035. doi:10.1016/j.ijpvp.2019.104035.
21. Kawasaki, Y.; Wakuda, T.; Kobarai, T.; Ohtsu, M. Corrosion Mechanisms in Reinforced Concrete by Acoustic Emission. *Construction and Building Materials* **2013**, *48*, 1240–1247. doi:10.1016/j.conbuildmat.2013.02.020.
22. Zaki, A.; Chai, H.K.; Aggelis, D.G.; Alver, N. Non-Destructive Evaluation for Corrosion Monitoring in Concrete: A Review and Capability of Acoustic Emission Technique. *Sensors* **2015**, *15*, 19069–19101. doi:10.3390/s150819069.

23. Idrissi, H.; Derenne, J.; Mazille, H. Detection of Pitting Corrosion of Aluminium Alloys by Acoustic Emission Technique. *J. Acoust. Emiss* **2000**, *18*, 409–416.
24. Bellenger, F.; Mazille, H.; Idrissi, H. Use of Acoustic Emission Technique for the Early Detection of Aluminum Alloys Exfoliation Corrosion. *NDT & E International* **2002**, *35*, 385–392. doi:10.1016/S0963-8695(02)00011-7.
25. Krakowiak, S.; Darowicki, K. Electrochemical and Acoustic Emission Studies of Aluminum Pitting Corrosion. *Journal of Solid State Electrochemistry* **2009**, *13*, 1653–1657. doi:10.1007/s10008-008-0759-0.
26. Pantelakis, S.; Setsika, D.; Chamos, A.; Zervaki, A. Corrosion Damage Evolution of the Aircraft Aluminum Alloy 2024 T3. *International Journal of Structural Integrity* **2016**, *7*, 25–46. doi:10.1108/IJSI-03-2014-0010.
27. Ostermann, F. *Anwendungstechnologie Aluminium*; Springer Berlin Heidelberg: Berlin, Heidelberg, 2014. doi:10.1007/978-3-662-43807-7.
28. Grosse, C.; Ohtsu, M., Eds. *Acoustic Emission Testing*; Springer Berlin Heidelberg: Berlin, Heidelberg, 2008. doi:10.1007/978-3-540-69972-9.
29. Giurgiutiu, V. *Structural Health Monitoring with Piezoelectric Wafer Active Sensors*; Academic Press, an imprint of Elsevier: Amsterdam, 2014.
30. Bhuiyan, M.Y.; Giurgiutiu, V. Multiphysics Simulation of Low-Amplitude Acoustic Wave Detection by Piezoelectric Wafer Active Sensors Validated by In-Situ AE-Fatigue Experiment. *Materials* **2017**, *10*, 962. doi:10.3390/ma10080962.
31. Mei, H.; Haider, M.F.; Joseph, R.; Migot, A.; Giurgiutiu, V. Recent Advances in Piezoelectric Wafer Active Sensors for Structural Health Monitoring Applications. *Sensors* **2019**, *19*, 383. doi:10.3390/s19020383.
32. Lu, Y.; Zhang, J.; Li, Z.; Dong, B. Corrosion Monitoring of Reinforced Concrete Beam Using Embedded Cement-Based Piezoelectric Sensor. *Magazine of Concrete Research* **2013**, *65*, 1265–1276. doi:10.1680/macr.13.00071.
33. Peng, C.; Chen, L.; Tang, M. A Database for Deliquescence and Efflorescence Relative Humidities of Compounds with Atmospheric Relevance. *Fundamental Research* **2021**. doi:10.1016/j.fmre.2021.11.021.
34. Winston, P.W.; Bates, D.H. Saturated Solutions For the Control of Humidity in Biological Research. *Ecology* **1960**, *41*, 232–237. doi:10.2307/1931961.
35. Barat, V.; Borodin, Y.; Kuzmin, A. Intelligent AE Signal Filtering Methods. *Journal of Acoustic Emission* **2010**, *28*, 109–120.